Hindawi Publishing Corporation
Journal of Nanomaterials
Volume 2014, Article ID 739251, 8 pages
http://dx.doi.org/10.1155/2014/739251

Research Article

Photocatalysis of WO_3 Nanoplates Synthesized by Conventional-Hydrothermal and Microwave-Hydrothermal Methods and of Commercial WO_3 Nanorods

Jarupat Sungpanich,[1] Titipun Thongtem,[2,3] and Somchai Thongtem[1,3]

[1] *Department of Physics and Materials Science, Faculty of Science, Chiang Mai University, Chiang Mai 50200, Thailand*
[2] *Department of Chemistry, Faculty of Science, Chiang Mai University, Chiang Mai 50200, Thailand*
[3] *Materials Science Research Center, Faculty of Science, Chiang Mai University, Chiang Mai 50200, Thailand*

Correspondence should be addressed to Titipun Thongtem; ttpthongtem@yahoo.com
and Somchai Thongtem; schthongtem@yahoo.com

Received 6 May 2014; Accepted 5 July 2014; Published 7 August 2014

Academic Editor: Sheng-Rui Jian

The degradation of methylene blue (MB) dye by tungsten oxide (WO_3) photocatalyst synthesized by the 200°C conventional-hydrothermal (C-H) and 270 W microwave-hydrothermal (M-H) methods and commercial WO_3 was studied under UV light irradiation for 360 min. The photocatalysts were characterized by X-ray diffraction (XRD), scanning electron microscopy (SEM), transmission electron microscopy (TEM), Fourier transform infrared (FTIR) spectroscopy, Raman spectrophotometry, and UV visible spectroscopy to determine phase, morphology, vibration mode, and optical property. The BET analysis revealed the specific surface area of 29.74, 37.25, and 33.56 m^2/g for the C-H WO_3 nanoplates, M-H WO_3 nanoplates, and commercial WO_3 nanorods, respectively. In this research, the M-H WO_3 nanoplates have the highest photocatalytic efficiency of 90.07% within 360 min, comparing to the C-H WO_3 nanoplates and even commercial WO_3 nanorods.

1. Introduction

In the past decade, nanostructured materials with zero-dimensional quantum dots, one-dimensional nanofibers, nanotubes, and nanorods, and two-dimensional nanoplates and nanodisks have been widely synthesized and studied of their novel properties which are different from their counterparts [1]. Particularly, transition metal oxide based nanostructured semiconductors have become a rapid expansion in modern materials science, physics, and chemistry [2, 3]. Tungsten oxide is an *n*-type semiconductor having attractive properties, especially as photochromic and electrochromic materials, and novel potential applications for using as gas sensors [3–5], humidity sensors [6], electrochromic devices [7], and photocatalysts [1, 5, 8, 9]. During the last several decades, nanostructured WO_3 has been synthesized by different processes: hydrothermal method [5, 9, 10], microwave radiation [11], microwave plasma [12], microwave-assisted hydrothermal synthesis [8, 13], and sol-gel [6, 7]. Most previous approaches to the synthesis of WO_3 nanomaterials such as conventional-hydrothermal and microwave-hydrothermal methods have several advantages. Komarneni [14] reported that these methods consumed less energy and were cost-effective and environmental friendly, and that the products are high purified single crystal. Although the hydrothermal process is slow kinetics at any given temperature, a combination of microwave and hydrothermal systems has been used to increase the kinetics of crystallization [14]. Due to the environmental remedy and energy-saving, photocatalytic semiconductors have been carried out. Sun et al. [15] described two main limitations for the wide use of the semiconductors: the low solar energy conversion efficiency due to their wide band gap and the high recombination rate of photo-induced electron-hole pairs. WO_3 as one of the photocatalytic materials has been extensively investigated, mainly due to its high activities for hydrogen evolution from water and degradation

of pollutants for water treatment [9, 16, 17]. The physical and chemical properties of the solid semiconductor surfaces are controlled by the synthesis method [18]. In the previous research [13], WO_3 nanoplates were successfully synthesized by a 270 W microwave-hydrothermal reaction for 180 min and the formation mechanism was also proposed according to the experimental results. At present, photocatalysis of WO_3 nanoplates synthesized by the conventional-hydrothermal (C-H) method at 200°C for 12 h, WO_3 nanoplates synthesized by the 270 W microwave-hydrothermal (M-H) method for 180 min [13], and commercial (com) WO_3 nanorods was investigated by determining the photodegradation of methylene blue (MB) dye under UV light irradiation.

2. Experimental Procedure

2.1. Synthesis. To synthesize WO_3 nanoplates, 1 mmol sodium tungstate ($Na_2WO_4{\cdot}2H_2O$, 99.0%) and 0.2 g citric acid ($C_6H_8O_7{\cdot}H_2O$) were dissolved in 40 mL deionized water with 10 min vigorous magnetic stirring till complete dissolution. Subsequently, 37% HCl was dropped to the solution until pH reaching 1. Then the solution was vigorously stirred by a magnetic stirrer for 30 min until the turbid yellow solution was obtained. Each of the turbid yellow solutions was transferred into Teflon lined stainless steel autoclaves, which were heated at 120, 160, and 200°C for 12 h. In the end, the autoclaves were naturally cooled to room temperature. The as-synthesized yellow precipitates were washed with ethanol and distilled water three times and dried at 80°C for 24 h for further studies. The system was also processed by the 270 W microwave-hydrothermal reaction for 180 min.

2.2. Characterization. The final products were characterized by Rigaku MiniFlex X-ray diffractometer with Cu-K_α radiation (λ = 1.54178 Å) ranging from 10° to 80°, in combination with database of the Joint Committee on Powder Diffraction Standards (JCPDS) [19]. The scanning electron microscopic (SEM) images were carried out by field emission scanning electron microscopy (JEOL JSM-6335F). Transmission electron microscopic (TEM) and high-resolution transmission electron microscopic (HRTEM) images and selected area electron diffraction (SAED) pattern were taken on a transmission electron microscope (JEOL JEM-2010) accelerating at a voltage of 200 kV. Fourier transform infrared (FTIR) spectra were recorded on a Bruker Tensor 27 spectrometer with KBr as a diluting agent and operated in the range of 400–4000 cm^{-1}. Raman spectra were recorded on a T64000 HORIBA Jobin Yvon spectrometer using a 50 mW and 514.5 nm wavelength Ar green laser. UV-visible absorption spectra were recorded on a Lambda 25 Perkin Elmer spectrometer using a UV lamp with 1 nm resolution ranging from 300 to 1000 nm. The Brunauer-Emmett-Teller (BET) surface area was determined by a Quantachrome Autosorb 1-MP.

2.3. Photocatalysis. Photocatalytic activities of the WO_3 nanoplates synthesized by the M-H and C-H methods and the commercial WO_3 (Merck) nanorods were tested in a methylene blue ($C_{16}H_{18}N_3SCI$, MB) aqueous media under UV radiation. The initial concentration of 100 mL aqueous MB solution was set as 1×10^{-5} mol/L and loaded with 0.1 g WO_3. The suspension was irradiated by a 18 W UV lamp with the average light intensity of 50.7 W/m^2. The concentration of MB was traced by UV-visible spectroscopy (Lambda 25 Perkin Elmer) in the range of 450–900 nm and the absorbance at the characteristic band of 664 nm was used to determine MB concentration.

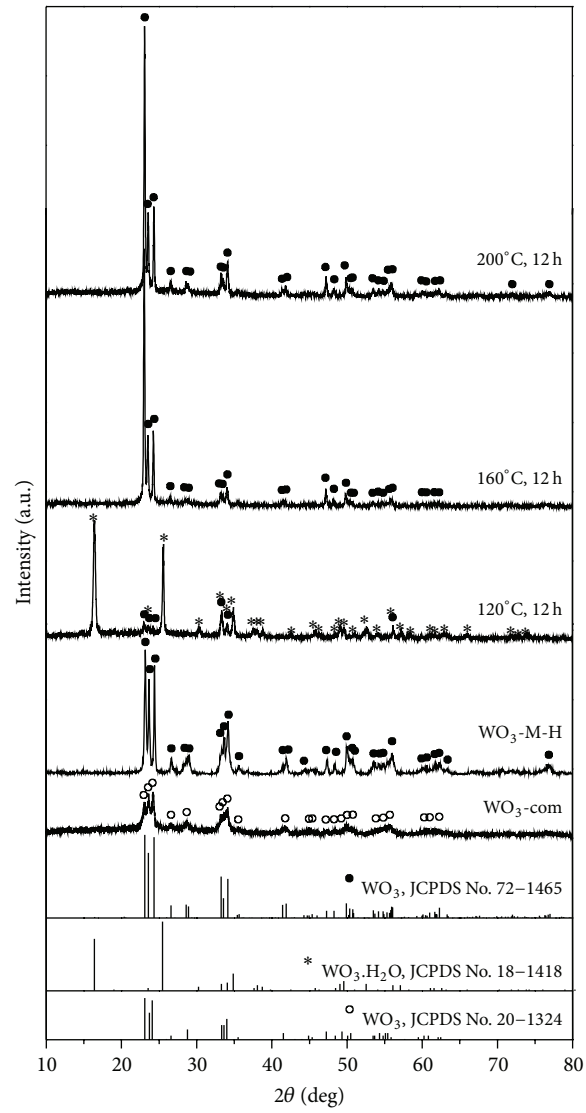

Figure 1: XRD patterns of the products synthesized by the C-H at 120, 160, and 200°C for 12 h and M-H at 270 W for 180 min and commercial (com) WO_3.

3. Results and Discussion

3.1. XRD. Comparing XRD spectra (Figure 1) of the products synthesized by the C-H method at 120, 160, and 200°C for 12 h with the JCPDS database (WO_3, No. 72-1465) [19], they corresponded with pure monoclinic crystal system and P21/n

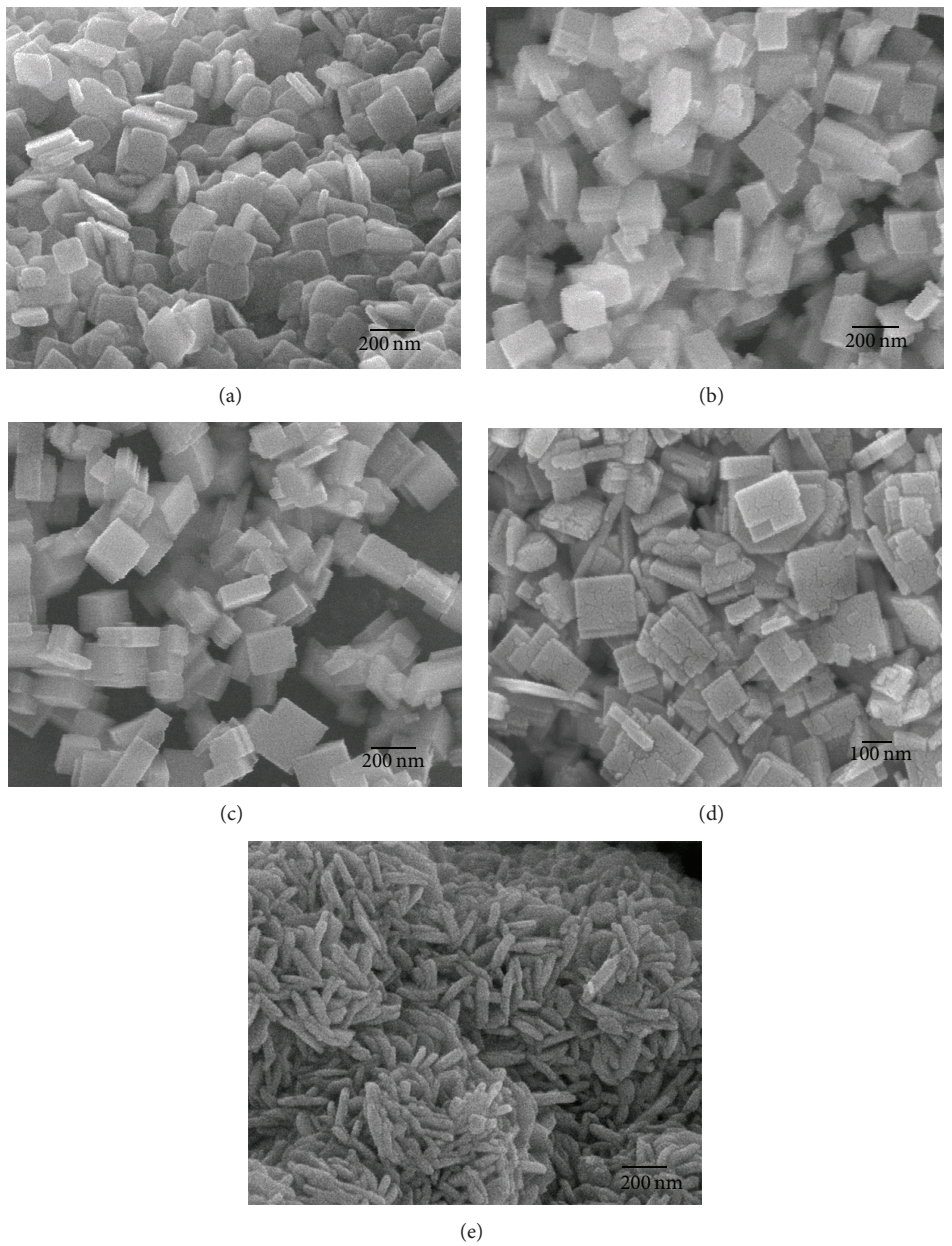

Figure 2: SEM images of the products, respectively, synthesized by the (a)–(c) C-H at 120, 160, and 200°C for 12 h and (d) M-H at 270 W for 180 min and (e) commercial WO_3.

space group at the synthesis temperatures of 160 and 200°C for 12 h. At 120°C, the product was composed of mixed phases of monoclinic WO_3 and orthorhombic $WO_3 \cdot H_2O$ (JCPDS No. 18-1418) [19]. Upon increasing the operation temperature to 160 and 200°C, pure monoclinic phase of WO_3 was detected. Their XRD intensity peaks were strengthened in sequence with the increase in the test temperature from 160°C to 200°C. In addition, the diffraction peaks of WO_3 synthesized by 270 W microwave-hydrothermal processed for 180 min [13] are also identical to the monoclinic phase of the JCPDS No. 72-1465 [19]. For commercial WO_3, the XRD pattern confirmed that the powder was composed of orthorhombic phase of WO_3 (JCPDS No. 20-1324) [19].

3.2. SEM. Morphologies of the products synthesized at 120, 160, and 200°C for 12 h were characterized by SEM as shown in Figures 2(a)–2(c). It can be clearly seen that irregular nanoplates of the products gradually transformed into completely rectangular shape by increasing the synthesis temperature. The particles were randomly oriented in different directions as those of the previous report [13]. The C-H synthesis surface of WO_3 was smoother than the M-H synthesis one (Figure 2(d)). Some traces of cracks were also detected on the M-H rectangular nanoplates. These cracks can play the role in promoting the product porosity. In this research, the C-H nanoplates are 50–100 nm thick, thicker than WO_3 nanoplates of the M-H. These imply that stability

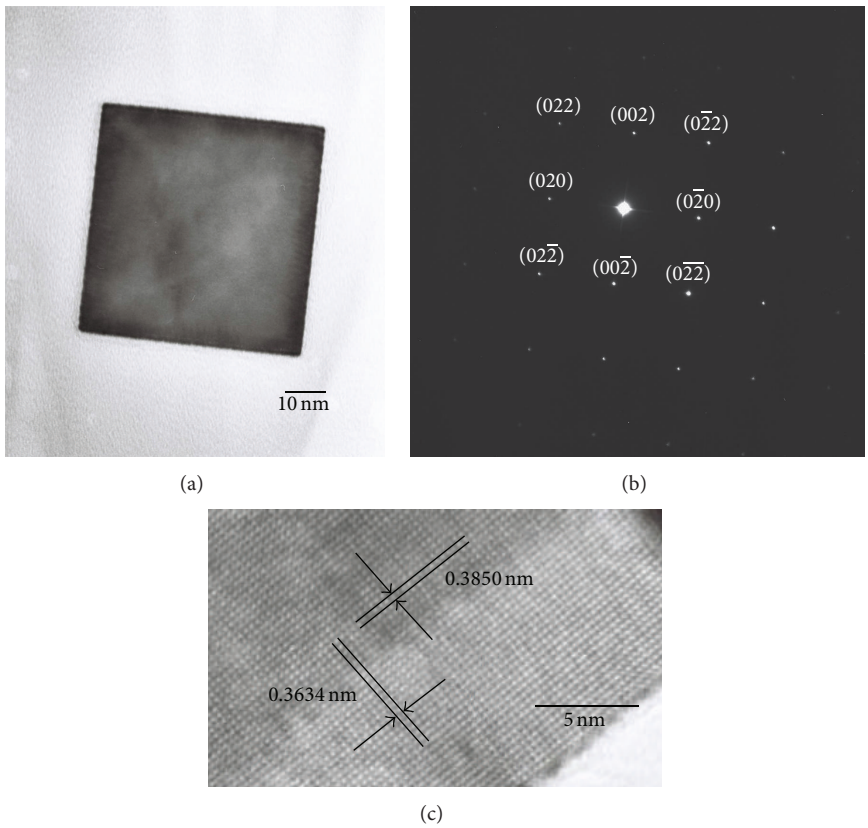

Figure 3: (a) TEM image, (b) SAED pattern, and (c) HRTEM image of WO_3 synthesized by the C-H at 200°C for 12 h.

of the pressure, temperature, and prolonged time can play a role in the crystal growth. The growth mechanism can be explained as follows: tiny nuclei formed by the reaction of $Na_2WO_4{\cdot}2H_2O$ and $C_6H_8O_7{\cdot}H_2O$ in the solution with the pH of 1 and grew as orthorhombic $WO_3{\cdot}H_2O$ irregular nanoplates at 120°C. By increasing the temperature to 160 and 200°C, monoclinic WO_3 rectangular nanoplates with anisotropic growth rate were detected, especially, at 200°C. It should be noted that the growth of WO_3 nanoparticles could be changed during phase transformation and was controlled by citric acid [13]. The SEM image of commercial WO_3 was also shown in Figure 2(e). It was composed of nanoparticles clustered together in the shape of nanorods with <100 nm diameter and ~200 nm length.

3.3. TEM. The morphology and phase of the product synthesized by the C-H at 200°C for 12 h were characterized by TEM, HRTEM, and SAED and are shown in Figure 3. In this research, the WO_3 product was shaped like rectangular nanoplates with the width and length of several 10 nm. SAED pattern of the product was indexed [19] to correspond with the (0 2 2), (0 0 2), (0 −2 2), (0 −2 0), (0 −2 −2), (0 0 −2), (0 2 −2), and (0 2 0) planes, specified as single crystalline WO_3 [19]. The electron beam was in the [1 0 0] direction. The HRTEM image of the product revealed the presence of lattice plane separation of 0.3850 nm and 0.3634 nm corresponding to the interlayer stacking of the (0 0 2) and (2 0 0) crystallographic planes of WO_3 (JCPDS No. 72-1465) [19], respectively.

3.4. FTIR. The FTIR spectra (Figure 4(a)) provided further insight into the structure of the products synthesized by the C-H at different temperatures for 12 h and commercial WO_3. At 120°C synthesis, the major vibration modes associated with O–H stretching of residual water was detected at 3655–3122 cm^{-1}, C=O stretching modes at 1626 cm^{-1}, C–O stretching modes of carboxyl at 948 cm^{-1}, O–W–O stretching modes at 814 and 746 cm^{-1}, and W–O–W stretching modes at 669 cm^{-1} [20–23]. Upon increasing the temperature from 120°C to 160°C and 200°C, the O–H and C=O stretching modes were no longer detected. For commercial WO_3, the observed peak was assigned to W–O bonding.

3.5. Raman Analysis. A definite existence of the products synthesized by the C-H at different temperatures for 12 h and commercial WO_3 was revealed by Raman analysis (Figure 4(b)). For WO_3 synthesized at 160 and 200°C and commercial WO_3, two main peaks are typical O–W–O stretching modes of crystalline WO_3 at 802 cm^{-1} (symmetric) for the shorter bonds, and 712 cm^{-1} (asymmetric) for the longer ones. Weak peaks at 610 cm^{-1} are assigned as the O–W–O stretching modes of WO_3. Those at 325, 273, and 241 cm^{-1} are specified as W–O–W bending modes of the

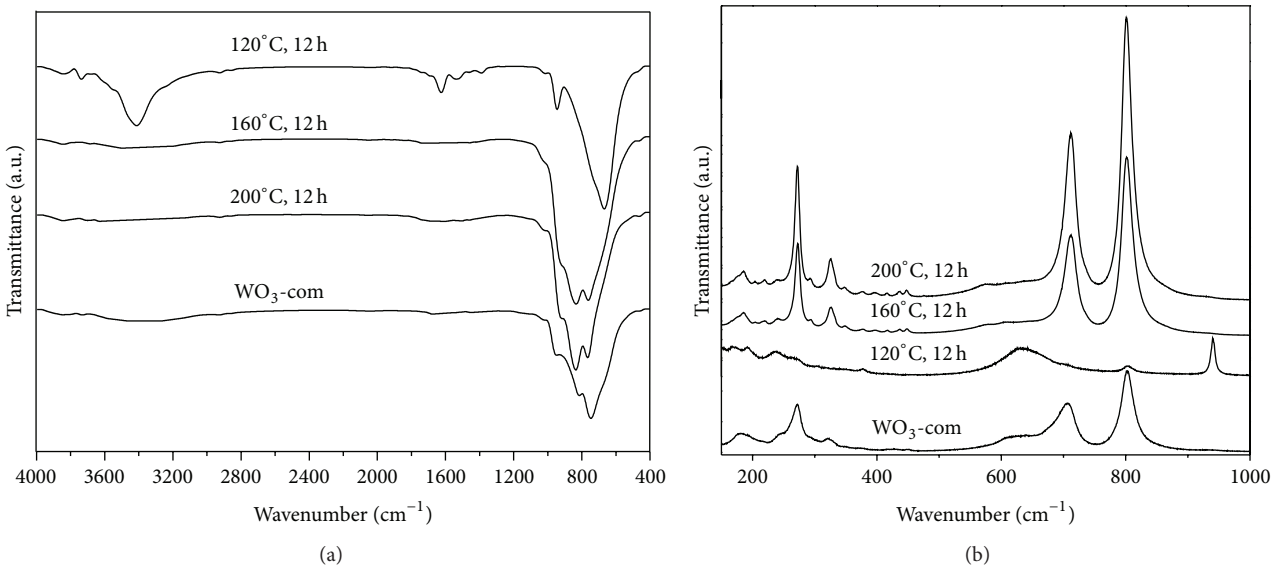

Figure 4: (a) FTIR and (b) Raman spectra of the products synthesized by the C-H at 120, 160, and 200°C for 12 h and commercial WO_3.

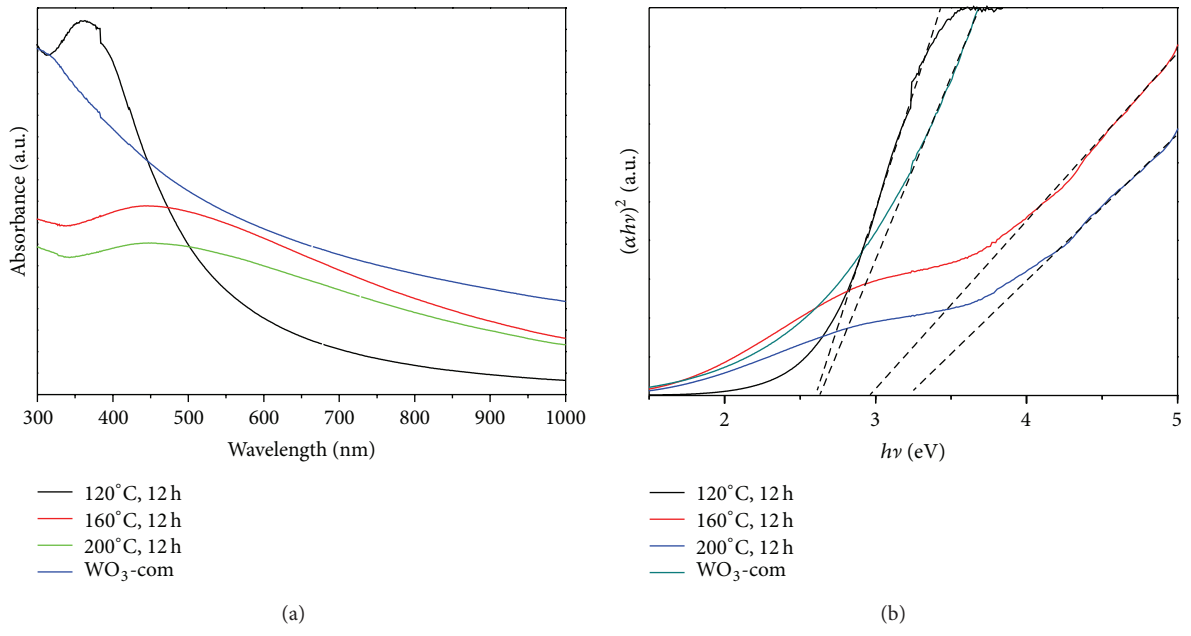

Figure 5: (a) UV-visible absorption and (b) the plot of $(\alpha h\nu)^2$ versus $h\nu$ of the products synthesized by the C-H at 120, 160, and 200°C for 12 h and commercial WO_3.

bridging oxygen. The peaks at 186 cm^{-1} are attributed to the lattice vibration. Additional mode belonging to W=O stretching of the product processed at 120°C for 12 h was also detected at 940 cm^{-1} [20, 23–27].

3.6. UV-Visible Absorption. UV-visible absorption of the products synthesized by the C-H at different temperatures for 12 h and commercial WO_3 is shown in Figure 5. For crystalline semiconductors, the UV absorption near band edge follows the following Wood and Tauc equation [28]:

$$\alpha h\nu = \left(h\nu - E_g\right)^n, \quad (1)$$

where α is the absorbance, h is the Planck constant, ν is the photon frequency, E_g is the energy gap, and n is a pure number associated with the different types of charged

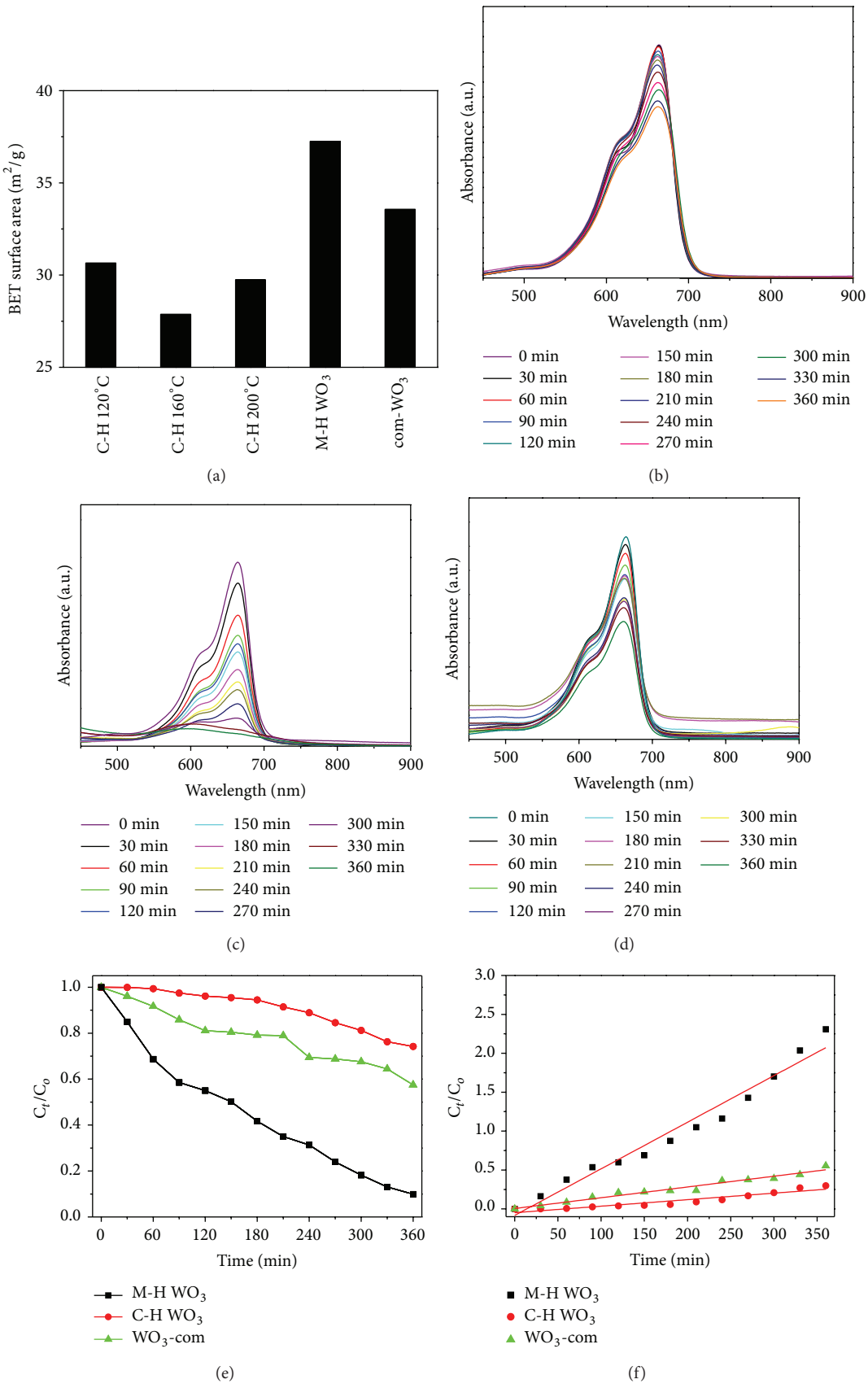

Figure 6: (a) BET surface areas of the products synthesized by the C-H at 120, 160, and 200°C for 12 h and M-H at 270 W for 180 min and commercial (com) WO_3. (b)–(d) UV-visible absorption spectra and (e), (f) photocatalytic degradation kinetics of MB dye by the WO_3 photocatalysts of the 200°C C-H and 270 W M-H and the commercial WO_3 irradiated with UV light for different lengths of time.

transition. The transitions are directly allowed, indirectly allowed, directly forbidden, and indirectly forbidden for n equals 1/2, 2, 3/2, and 3, respectively. The absorption was controlled by two photon energy ranges relative to energy gap. For $h\nu > E_g$, absorption is linearly increased with the increasing of photon energy caused by the transition of electrons from the topmost occupied state of valence band to the bottommost unoccupied state of conduction band. For $h\nu < E_g$, the absorption curves are different from linearity, caused by charged transition relating to defects. In the present research, direct energy gaps of the products synthesized by the C-H at 120, 160, and 200°C for 12 h were determined to be 2.60, 2.96, and 3.22 eV, respectively [2, 29, 30]. In addition, the direct band gap of commercial WO_3 was determined to be 2.63 eV [8].

3.7. BET Analysis. The BET analysis was used to determine surface area of the products (Figure 6(a)). It was found that pure WO_3 of the M-H (37.25 m^2/g) has larger surface area than the product of the C-H and commercial WO_3 (33.56 m^2/g). Surface area of the product synthesized by the C-H at 120°C for 12 h ($WO_3 \cdot H_2O$) was determined to be 30.65 m^2/g. Pure WO_3 products at 160 and 200°C for 12 h were determined to be 27.87 and 29.74 m^2/g, respectively. The M-H processed WO_3 nanostructure has different size distributions due to thermal stress during rapid heating, and the M-H product is also shown as rough surface. The traces of cracks on the M-H nanoplates and small debris separation have the influence to increase surface area.

3.8. Photocatalysis. The photocatalytic activities of WO_3 synthesized by the 200°C C-H and 270 W M-H and of the commercial WO_3 photocatalyst were evaluated by identifying the degradation of methylene blue ($C_{16}H_{18}N_3SCI$, MB) under UV radiation. Before UV irradiation, 100 mL of 1×10^{-5} mol/L MB aqueous solution containing 0.1 g of photocatalyst was magnetically stirred in the dark for 30 min. For comparison, WO_3 synthesized by the 200°C of the C-H for 12 h, WO_3 of the 270 W M-H for 180 min, and commercial WO_3 were used as photocatalytic materials for degrading MB under UV radiation. Figures 6(b)–6(d) show the UV-visible absorption spectra of MB in aqueous solution containing WO_3 synthesized by the C-H and M-H methods and commercial WO_3 for different lengths of irradiation time. The characteristic absorption peaks of MB at 664 nm gradually decrease with the prolonging irradiation time. For WO_3 photocatalyst of the M-H, the characteristic absorption peak decreases almost disappear within 360 min. The MB degradation under a series of the experimental conditions is shown in Figure 6(e), where C_o and C_t are the initial concentration after the equilibrium absorption and residual concentration of MB within the length of time (t), respectively. The MB concentration of WO_3 photocatalyst of the C-H decreases slower than WO_3 of the M-H and commercial one under UV radiation. The degradation efficiencies for the M-H, commercial, and C-H photocatalysts were 90.07%, 42.53%, and 25.80% within 360 min irradiation, respectively. These results corresponded with the BET analysis. Not only surface area plays the role in the photocatalytic activity but the crystalline composition of the photocatalyst also shows an important effect [31]. The crystalline structure and morphology of the M-H and C-H WO_3 (monoclinic, nanoplates) are difference from those of commercial WO_3 (orthorhombic, nanorods). They also have the influence to control the photocatalytic rate. The Langmuir-Hinshelwood (L-H) kinetics model was used to investigate the degradation of MB solution and the pseudo-first-order rate equation was given by [18]

$$\ln\left(\frac{C_o}{C_t}\right) = k_{\text{app}}t, \tag{2}$$

where C_o is the equilibrium concentration after absorption, C_t is the concentration of MB at time t, and k_{app} represents the apparent pseudo-first-order rate constant of initial degradation. The pseudo-first-order rate constant (k_{app}) was calculated from the slope of the $\ln(C_o/C_t)$ versus irradiation time (t) shown in Figure 6(f). The rate constant of MB degradation was 0.00599 min^{-1}, 8.38072×10^{-4} min^{-1}, and 0.00138 min^{-1} in the solutions containing the M-H WO_3, C-H WO_3, and commercial WO_3, respectively.

4. Conclusions

In summary, WO_3 nanoplates were successfully synthesized by the citric acid-assisted conventional hydrothermal reaction at 200°C for 12 h. Phase, morphology, and optical properties of the products were investigated. The photocatalytic property of the C-H WO_3 was evaluated by identifying the degradation of MB dye under UV irradiation and compared with the M-H WO_3 and commercial WO_3. The results indicated that the M-H WO_3 nanoplates showed the highest efficiency for the degradation of MB dye at the rate of 90.07% under UV illumination within 360 min, corresponding to the BET surface area analysis.

Conflict of Interests

The authors declare that there is no conflict of interests regarding the publication of this paper.

Acknowledgments

The authors wish to thank the Thailand Research Fund (TRF) for providing financial support through the Royal Golden Jubilee Ph.D. Program and the TRF Research Grant BRG5380020; the National Nanotechnology Center (NANOTEC), National Science and Technology Development Agency (NSTDA), Thailand, through the project P-10-11345 for Research, Development and Engineering (RD & E); and the Thailand's Office of the Higher Education Commission through the National Research University (NRU) Project for Chiang Mai University (CMU), including the Graduate School of CMU through a general support.

References

[1] L. Li, J. Zhao, Y. Wang et al., "Oxalic acid mediated synthesis of $WO_3 \cdot H_2O$ nanoplates and self-assembled nanoflowers under mild conditions," *Journal of Solid State Chemistry*, vol. 184, no. 7, pp. 1661–1665, 2011.

[2] V. Hariharan, S. Radhakrishnan, M. Parthibavarman, R. Dhilipkumar, and C. Sekar, "Synthesis of polyethylene glycol (PEG) assisted tungsten oxide (WO_3) nanoparticles for l-dopa biosensing applications," *Talanta*, vol. 85, no. 4, pp. 2166–2174, 2011.

[3] J. Polleux, A. Gurlo, N. Barsan, U. Weimar, M. Antonietti, and M. Niederberger, "Template-free synthesis and assembly of single-crystalline tungsten oxide nanowires and their gas-sensing properties," *Angewandte Chemie International Edition*, vol. 45, no. 2, pp. 261–265, 2005.

[4] J. Shi, G. Hu, Y. Sun et al., "WO_3 nanocrystals: synthesis and application in highly sensitive detection of acetone," *Sensors and Actuators B: Chemical*, vol. 156, no. 2, pp. 820–824, 2011.

[5] X. Gao, X. Su, C. Yang et al., "Hydrothermal synthesis of WO_3 nanoplates as highly sensitive cyclohexene sensor and high-efficiency MB photocatalyst," *Sensors and Actuators B*, vol. 181, pp. 537–543, 2013.

[6] C. Dai, M. Liu, F. Chen, C. Wu, and M. Chang, "A nanowire WO_3 humidity sensor integrated with micro-heater and inverting amplifier circuit on chip manufactured using CMOS-MEMS technique," *Sensors and Actuators, B: Chemical*, vol. 123, no. 2, pp. 896–901, 2007.

[7] A. Danine, L. Cojocaru, C. Faure et al., "Room temperature UV treated WO_3 thin films for electrochromic devices on paper substrate," *Electrochimica Acta*, vol. 129, pp. 113–119, 2014.

[8] D. B. Hernandez-Uresti, D. Sánchez-Martínez, A. Martínez-delaCruz, S. Sepúlveda-Guzmán, and L. M. Torres- Martínez, "Characterization and photocatalytic properties of hexagonal and monoclinic WO_3 prepared via microwave-assisted hydrothermal synthesis," *Ceramics International*, vol. 40, no. 3, pp. 4767–4775, 2014.

[9] S. S. Thind, M. Tian, and A. Chen, "Direct growth and photoelectrochemical study of WO_3 nanostructured materials," *Electrochemistry Communications*, vol. 43, pp. 13–17, 2014.

[10] Z. Gu, T. Zhai, B. Gao et al., "Controllable assembly of WO_3 nanorods/nanowires into hierarchical nanostructures," *Journal of Physical Chemistry B*, vol. 110, no. 47, pp. 23829–23836, 2006.

[11] K. O. Rocha and S. M. Zanetti, "Structural and properties of nanocrystalline WO_3/TiO_2-based humidity sensors elements prepared by high energy activation," *Sensors and Actuators B: Chemical*, vol. 157, no. 2, pp. 654–661, 2011.

[12] K. Murugan, S. B. Chandrasekhar, and J. Joardar, "Nanostructured α/β-tungsten by reduction of WO_3 under microwave plasma," *International Journal of Refractory Metals and Hard Materials*, vol. 29, no. 1, pp. 128–133, 2011.

[13] J. Sungpanich, T. Thongtem, and S. Thongtem, "Large-scale synthesis of WO_3 nanoplates by a microwave-hydrothermal method," *Ceramics International*, vol. 38, no. 2, pp. 1051–1055, 2012.

[14] S. Komarneni, "Nanophase materials by hydrothermal, microwave-hydrothermal and microwave-solvothermal methods," *Current Science*, vol. 85, no. 12, pp. 1730–1734, 2003.

[15] L. Sun, X. Zhao, C. Jia et al., "Enhanced visible-light photocatalytic activity of g-C_3N_4-ZnWO4 by fabricating a heterojunction: investigation based on experimental and theoretical studies," *Journal of Materials Chemistry*, vol. 22, no. 44, pp. 23428–23438, 2012.

[16] S. Nishimoto, T. Mano, Y. Kameshima, and M. Miyake, "Photocatalytic water treatment over WO_3 under visible light irradiation combined with ozonation," *Chemical Physics Letters*, vol. 500, no. 1–3, pp. 86–89, 2010.

[17] W. Chu and Y. F. Rao, "Photocatalytic oxidation of monuron in the suspension of WO_3 under the irradiation of UV-visible light," *Chemosphere*, vol. 86, no. 11, pp. 1079–1086, 2012.

[18] N. A. Ramos-Delgadoa, M. A. Gracia-Pinillab, L. Maya-Treviño, L. Hinojosa-Reyesa, J. L. Guzman-Mara, and A. Hernández-Ramírez, "Solar photocatalytic activity of TiO_2 modified with WO_3 on thedegradation of an organophosphorus pesticide," *Journal of Hazardous Materials*, vol. 263, pp. 36–44, 2013.

[19] "Powder Diffraction File, JCPDS-ICDD," 12 Campus Boulevard, Newtown Square, Pa, USA, 2001.

[20] B. Ingham, S. V. Chong, and J. L. Tallon, "Layered tungsten oxide-based organic—Inorganic hybrid materials: an infrared and raman study," *Journal of Physical Chemistry B*, vol. 109, no. 11, pp. 4936–4940, 2005.

[21] H. S. Mansur, C. M. Sadahira, A. N. Souza, and A. A. P. Mansur, "FTIR spectroscopy characterization of poly (vinyl alcohol) hydrogel with different hydrolysis degree and chemically crosslinked with glutaraldehyde," *Materials Science and Engineering C*, vol. 28, no. 4, pp. 539–548, 2008.

[22] H. S. Mansur, R. L. Oréfice, and A. A. P. Mansur, "Characterization of poly(vinyl alcohol)/poly(ethylene glycol) hydrogels and PVA-derived hybrids by small-angle X-ray scattering and FTIR spectroscopy," *Polymer*, vol. 45, no. 21, pp. 7193–7202, 2004.

[23] S. Salmaoui, F. Sediri, and N. Gharbi, "Characterization of h-WO_3 nanorods synthesized by hydrothermal process," *Polyhedron*, vol. 29, no. 7, pp. 1771–1775, 2010.

[24] A. Kuzmin, J. Purans, E. Cazzanelli, C. Vinegoni, and G. Mariotto, "X-ray diffraction, extended x-ray absorption fine structure and Raman spectroscopy studies of WO_3 powders and $(1\text{-}x)WO_3\text{-}y\cdot xReO_2$ mixtures," *Journal of Applied Physics*, vol. 84, no. 10, pp. 5515–5524, 1998.

[25] C. S. Rout, M. Hegde, and C. N. R. Rao, "H_2S sensors based on tungsten oxide nanostructures," *Sensors and Actuators B: Chemical*, vol. 128, no. 2, pp. 488–493, 2008.

[26] T. Siciliano, A. Tepore, G. Micocci, A. Serra, D. Manno, and E. Filippo, "WO_3 gas sensors prepared by thermal oxidization of tungsten," *Sensors and Actuators, B: Chemical*, vol. 133, no. 1, pp. 321–326, 2008.

[27] Y. S. Kim, "Thermal treatment effects on the material and gas-sensing properties of room-temperature tungsten oxide nanorod sensors," *Sensors and Actuators B*, vol. 137, no. 1, pp. 297–304, 2009.

[28] Y. Keereeta, T. Thongtem, and S. Thongtem, "Fabrication of $ZnWO_4$ nanofibers by a high direct voltage electrospinning process," *Journal of Alloys and Compounds*, vol. 509, no. 23, pp. 6689–6695, 2011.

[29] Y. Shen, D. Ding, and Y. Deng, "Fabrication and characterization of WO_3 flocky microspheres induced by ethanol," *Powder Technology*, vol. 211, no. 1, pp. 114–119, 2011.

[30] K. Lee, W. S. Seo, and J. T. Park, "Synthesis and optical properties of colloidal tungsten oxide nanorods," *Journal of the American Chemical Society*, vol. 125, no. 12, pp. 3408–3409, 2003.

[31] M. Lindner, J. Theurich, and D. W. Bahnemann, "Photocatalytic degradation of organic compounds: accelerating the process efficiency," *Water Science and Technology*, vol. 35, no. 4, pp. 79–86, 1997.